Identification of an endocannabinoid gut-brain vagal mechanism controlling food reward and energy homeostasis

Chloé Berland[1], Julien Castel[1], Romano Terrasi[2], Enrica Montalban[1], Ewout Foppen[1], Claire Martin[1], Giulio G. Muccioli[2], Serge Luquet[1], Giuseppe Gangarossa[1]

[1] Université de Paris, BFA, UMR 8251, CNRS, F-75013 Paris, France

[2] Bioanalysis and Pharmacology of Bioactive Lipids Research Group, Louvain Drug Research Institute, Université catholique de Louvain, 1200 Brussels, Belgium

Correspondence to: giuseppe.gangarossa@u-paris.fr (GG, @PeppeGanga)

Running title: Peripheral endocannabinoids gate reward feeding and homeostasis

Key words: binge eating, dopamine, 2-AG, vagus nerve, striatum, reward, metabolism

Abstract (234)

The regulation of food intake, a *sine qua non* requirement for survival, thoroughly shapes feeding and energy balance by integrating both homeostatic and hedonic values of food. Unfortunately, the widespread access to palatable food has led to the development of feeding habits that are independent from metabolic needs. Among these, binge eating (BE) is characterized by uncontrolled voracious eating. While reward deficit seems to be a major contributor of BE, the physiological and molecular underpinnings of BE establishment remain elusive. Here, we combined a physiologically relevant BE mouse model with multiscale *in vivo* approaches to explore the functional connection between the gut-brain axis and the reward and homeostatic brain structures.

Our results show that BE elicits compensatory adaptations requiring the gut-to-brain axis which, through the vagus nerve, relies on the permissive actions of peripheral endocannabinoids (eCBs) signaling. Selective inhibition of peripheral CB1 receptors resulted in a vagus-dependent increased hypothalamic activity, modified metabolic efficiency, and dampened activity of mesolimbic dopamine circuit, altogether leading to the suppression of palatable eating. We provide compelling evidence for a yet unappreciated physiological integrative mechanism by which variations of peripheral eCBs control the activity of the vagus nerve, thereby in turn gating the additive responses of both homeostatic and hedonic brain circuits which govern homeostatic and reward-driven feeding.

In conclusion, we reveal that vagus-mediated eCBs/CB1R functions represent an interesting and innovative target to modulate energy balance and counteract food-reward disorders.

Introduction

Feeding is a complex and highly conserved process whose orchestration results from the dynamic integration of interoceptive and exteroceptive signals. The homeostatic and hedonic components of feeding have been attributed to the hypothalamus and the dopamine (DA) reward system, respectively [1]. While the firsts can be broadly defined as key regulators of food intake to ensure optimal energy balance, the seconds mainly relate to the reinforcing properties of sensory stimuli (perception, cues, taste, odors) and reward-associated features of feeding. However, despite the well-accepted recognition that both feeding components are tightly and functionally interconnected [1], they are usually investigated as isolated systems. In addition, the counterpointing central *vs* peripheral regulations of feeding add a supplemental degree of complexity in the identification of integrative regulatory mechanisms [2].

While energy homeostasis refers to negative feedback mechanisms maintaining body weight at *set-points*, the combination of both homeostatic and hedonic components of feeding leads to the establishment of feed-forward mechanisms of physiological adaptations. Feed-forward adaptation, also known as allostasis (*stability through changes*), is critical for energy balance and metabolic efficiency [3] but also contributes to reward-associated events [4]. Indeed, the widespread availability and consumption of palatable diets have profoundly altered the delicate allostatic integration of homeostatic and hedonic signals, leading to the development of metabolic disorders. This is particularly evident in food reward-driven dysfunctions such as binge eating (BE), where uncontrolled feeding perfectly recapitulates the efforts for an organism to adapt its homeostatic processes to the hedonic aspects of feeding. In fact, short- and/or long-term consumptions of energy-rich palatable diets remodel the DA reward system [5] and promote functional adaptations within the hypothalamus [6–8]. Beyond these two core processors of feeding, recent reports have mechanistically demonstrated that the gut-brain vagal axis, besides sensing interoceptive signals and influencing feeding and energy homeostasis [9–11], is also a major modulator of the reward system [12–14]. However, the physiological processes by which the gut-to-brain axis modulates reward feeding remain unclear. Emerging evidence strongly suggest that, besides a plethora of peripheral hormones (*i.e.* ghrelin, leptin, GLP-1, CCK), peripheral endocannabinoids (eCBs) may be fundamental players in the regulation of feeding and metabolic efficiency [15–17].

Indeed, eating disorders-associated alterations in peripheral eCBs have been reported in obese and BE patients [18, 19] as well as in diet-induced obese rodents [15, 20]. However, whether and how peripheral eCBs play a permissive role in guiding reward-based feeding behaviors and in buffering the allostatic regulation of energy balance is unexplored.

To tackle this question, we took advantage of a physiologically relevant BE-like mouse paradigm which, by promoting anticipatory and escalated consummatory food responses, triggers reward-driven behavioral, molecular and allostatic adaptations. Binge eating, which elicited DA-dependent molecular modifications in the reward-related structures [dorsal striatum (DS) and nucleus accumbens (NAc)], revealed an unappreciated integrative gut-to-brain orchestration requiring the modulatory actions of peripheral eCBs. In particular, we show that BE requires an orchestrated dialog between peripheral eCBs and both central hypothalamic and VTA structures through the gut-brain vagal axis, thus modulating both energy balance and reward-like events.

Material and methods

See **Suppl. Material** for the detailed description of materials, methods and techniques, and experimental sizes used in the whole study.

Animals

All experiments were approved by the Animal Care Committee of the Université de Paris (CEB-25–2016) and carried out following the 2010/63/EU directive. 8-12 weeks old male and/or female C57Bl/6J mice (Janvier, Le Genest St Isle, France) were single-housed one week prior to any experimentation in a room maintained at 22 +/-1 °C, with light period from 7 AM to 7 PM. Regular chow diet (3 438 kcal/kg, protein 19%, fat 5%, carbohydrates 55%, of total kcal, reference #U8959 version 63 Safe, Augy, France) and water were provided *ad libitum*. *Drd2*-Cre mice [Tg(Drd2-cre) ER44Gsat/Mmucd, Jackson laboratory] were used for *in vivo* fiber photometry Ca^{2+} imaging in the VTA. *Drd2*-eGFP mice [Tg(Drd2-eGFP)S118Gsat/Mmnc] were generated by GENSAT at the Rockefeller University. See **Suppl. Material** for further details.

Behaviors

Palatable binge eating-like paradigm. Intermittent daily access to a palatable mixture (Intralipid 20% w/v + sucrose 10% w/v) was provided for 1-hour/day during 10-14 consecutive days at 10-11 AM in home-cages. During time-locked binge sessions regular chow pellets were not removed. Volume (mL) of consumed palatable mixture was measured at the end of the session.

Locomotor activity. Spontaneous and/or induced locomotor activities were measured using an infrared beam-based activity monitoring system (Phenomaster, TSE Systems GmbH, Germany).

Tail suspension. To record the activity of GCaMP6f-expressing VTA neurons, mice were suspended above the ground by their tails. Ca^{2+} imaging was performed before and during tail suspension.

Exploratory drive in a new environment. To record the activity of GCaMP6f-expressing VTA neurons in a novelty-induced exploratory drive, mice were put in a new environment (NE) consisting in a novel cage. Ca^{2+} imaging was performed before and immediately after changing the environment. See **Suppl. Material** for further details.

Metabolic efficiency analysis

Mice were monitored for whole energy expenditure (EE), O_2 consumption, CO_2 production, respiratory exchange rate (RER=VCO_2/VO_2, V=volume), and locomotor activity using calorimetric cages (Labmaster, TSE Systems GmbH, Bad Homburg, Germany). Ratio of gases was determined through an indirect open circuit calorimeter. This system monitors O_2 and CO_2 at the inlet ports of a tide cage through which a known flow of air is ventilated (0.4 L/min) and regularly compared to a reference empty cage. O_2 consumption and CO_2 production were recorded every 15 min during the entire experiment. EE was calculated using the Weir equation for respiratory gas exchange measurements. Food intake was measured with highly sensitive sensors for automated online measurements. Mice had access to food and water *ad libitum*. Mice were monitored for body weight and composition at the entry and exit of the experiment using an EchoMRI (Whole Body Composition Analyzers, EchoMRI, Houston, USA). Data analysis was performed on Excel XP using extracted raw values of VO_2, VCO_2 (mL/h), and EE (kcal/h).

Brown adipose tissue and telemetry body temperature measurements

Infrared camera for BAT temperature. Heat production was visualized using a high-resolution infrared camera (FLIR E8; FLIR Systems, Portland, OR, USA). To measure brown adipose tissue (BAT) temperature, images of interscapular regions were captured before and after binge sessions. Infrared thermography was analyzed using the FLIR TOOLS.

Telemetry body temperature. Anesthetized mice were implanted with a the telemetric transmitter (HD-XG; Data Sciences International) to measure longitudinal fluctuations of core temperature. They were allowed to recover at 35°C and received a daily injection of ketoprofen (Ketofen® 10%) for 3 days. During a 7-days recovery period, mice were monitored and had facilitated access to food. Data were collected using the Ponemah® software (DSI). The detection of transmitted signals was accomplished by a radio receiver (body temperature and locomotor activity) and processed by a microcomputer system.

Tissue preparation and immunofluorescence

Mice were anaesthetized with pentobarbital (500 mg/kg, i.p., Sanofi-Aventis, France) and transcardially perfused with 4°C PFA 4% for 5 minutes. Sections were processed as previously described [21]. Quantification of immunopositive cells was performed using the cell counter plugin of ImageJ software taking a fixed threshold of fluorescence as standard reference. See **Suppl. Material** for further details and list of antibodies.

Western blotting and quantitative RT-PCR

At the end of the binge session, the mouse head was cut and immediately immersed in liquid nitrogen for 3 seconds. Brains and sampled structures were processed as previously described [21]. Quantifications were performed using ImageJ software. See **Suppl. Material** for further details, list of antibodies and primers.

Drug treatments

The following compounds were used: insulin (0.5 U/kg, Novo Nordisk), CCK-8S (10 ug/kg, Tocris), liraglutide (100 ug/kg, gift from Novo Nordisk), exendin 4 (10 ug/kg, Tocris), leptin (twice/day for 2 days at 0.25 mg/kg, Tocris), AM251 (3 mg/kg, Tocris), AM6545 (10 mg/kg, Tocris), JD-5037 (3 mg/kg, MedChemExpress), SKF81297 (5 mg/kg, Tocris), haloperidol (0.25 and 0.5 mg/kg, Tocris), SCH23390 (0.1 mg/kg, Tocris), GBR12909 (10 mg/kg, Tocris), d-amphetamine sulphate (2 mg/kg, Tocris), JZL184 (8 mg/kg, Tocris). See **Suppl. Material** for further details.

Subdiaphragmatic vagotomy

Prior to surgery and during 3 post-surgery days, animals were provided with *ad libitum* jelly food (DietGel Boost #72-04-5022, Clear H_2O) to avoid the presence of solid food in the gastrointestinal tract. Animals received Buprécare® (Buprenorphine 0.3 mg) and Ketofen® (100 mg) and were anaesthetized with isoflurane (3.5% for induction, 1.5% for maintenance). Body temperature was maintained at 37°C. Briefly, using a binocular microscope, the right and left vagus nerve branches were carefully isolated along the esophagus and sectioned in vagotomized (VGX) animals or left intact in sham animals. Mice recovered for at least 3 weeks before being used for experimental procedures. See **Suppl. Material** for further details.

Quantification of eCBs by UHPLC-MS/MS

Lipids were extracted by liquid/liquid extraction in the presence of deuterated standards. They were then purified by SPE to obtain a fraction containing eCB and NAE that were analyzed by UHPLC-MS/MS using a Xevo TQ-S (ESI source; positive mode). For each analyte, the signal (AUC) of the relevant internal standard was used for normalization. See **Suppl. Material** for further details.

Viral production

pAAV.Syn.Flex.GCaMP6f.WPRE.SV40 (titer ≥ 1×10^{13} vg/ml, working dilution 1:5) was a gift from Douglas Kim (Addgene viral prep #100833-AAV9; http://n2t.net/addgene:100833; RRID:Addgene_100833).

pAAV5-hSyn-dLigh1.2 (titer ≥ 4×10^{12} vg/mL) was a gift from Lin Tian (Addgene viral prep #111068-AAV5; http://n2t.net/addgene:111068; RRID:Addgene_111068).

Stereotaxic procedure

Mice were anaesthetized with isoflurane, administered with Buprécare® (Buprenorphine 0.3 mg) and Ketofen® (Ketoprofen 100 mg), and placed on a stereotactic frame (Model 940, David Kopf Instruments, California). pAAV.Syn.Flex.GCaMP6f.WPRE.SV40 (0.3 µl) was injected unilaterally into the VTA (L=−0.5; AP=−3.4; V=−4.4, mm) of *Drd2*-Cre mice at a rate of 0.05 µl/min.

pAAV5-hSyn-dLight1.2 (0.5 µl) was injected unilaterally into the NAc (L=−0.75; AP=1.18; V=−4.4, mm) of C57BL6/J male and female mice at a rate of 0.05 µl/min.

The injection needle was carefully removed after 5 minutes waiting at the injection site and 2 minutes waiting halfway to the top. Optical fiber for Ca^{2+} (VTA) and dopamine (NAc) imaging was implanted 100 µm above the viral injection site. Animals were tested 4 weeks after viral stereotaxic injections.

Fiber photometry and data analysis

A chronically implantable cannula (Doric Lenses, Québec, Canada) composed of a bare optical fiber (400 µm core, 0.48 N.A.) and a fiber ferrule was implanted 100 µm above the location of the viral injection site in the VTA or in the NAc. The fiber was fixed onto the skull using dental cement (Super-Bond C&B, Sun Medical). Real-time fluorescence signals emitted by GCaMP6f or the DA biosensor dLight1.2 [22] were recorded and analyzed as previously described [21]. Fluorescence was collected using a single optical fiber for both delivery of excitation light streams and collection

of emitted fluorescence. The fiber photometry setup used 2 light-emitting LEDs: 405 nm LED sinusoidally modulated at 330 Hz and a 465 nm LED sinusoidally modulated at 533 Hz merged in a FMC4 MiniCube (Doric Lenses) that combines the 2 wavelengths excitation light streams and separate them from the emission light. The MiniCube was connected to a Fiberoptic rotary joint connected to the cannula. A RZ5P lock-in digital processor controlled by the Synapse software (Tucker-Davis Technologies, TDT, USA), commanded the voltage signal sent to the emitting LEDs via the LED driver (Doric Lenses). Data are presented as z-score of ΔF/F. See **Suppl. Material** for further details.

Statistics

All data are presented as mean ± SEM. Statistical tests were performed with Prism 7 (GraphPad Software, La Jolla, CA, USA). The detailed statistical analyses are listed in the **Suppl. Table 1**. Normality was assessed by the D'Agostino-Pearson test. Depending on the experimental design, data were analyzed using either Student t-test (paired or unpaired) with equal variances, One-way ANOVA or Two-way ANOVA. In all cases, the significance threshold was automatically set at $p < 0.05$. ANOVA analyses were followed by Bonferroni *post hoc* test for specific comparisons only when overall ANOVA revealed a significant difference (at least $p < 0.05$).

Results

Time-locked access to palatable diet induces adaptation of nutrient partitioning and metabolic efficiency

Several paradigms of bingeing are widely used to model eating disorders [23]. However, the majority of these paradigms mainly rely on (*i*) prior alterations of basal homeostasis (food or water restriction/deprivation, stress induction), (*ii*) dietary exposure to either high-sugar or high-fat foods, or (*iii*) absence of food choice during bingeing periods. We therefore adapted existing protocols to better study reward and homeostatic components of food intake during binge eating (BE). Since dietary mixtures of fat and sugar lead to enhanced food reward properties [24], we designed a highly palatable diet (sugar and fat) to promote intense reward-driven feeding. Time-locked access to this palatable diet was sufficient to drive escalating binge-like consumption without restricting access to chow diet (**Fig. 1A**). In that regard, we are confident that this model is preferentially driven by reward values over metabolic demands since animals are neither food nor water restricted.

Male mice intermittently exposed to this dietary palatable mixture maximized their intake within a few days (**Fig. 1B**). This palatable food consumption was simultaneously associated with an increased anticipatory locomotor activity ~2 hours before food access and lasted for another ~1-2 hours (**Fig. 1C, C^1**), with no changes in the ambulatory activity during the dark phase (**Fig. 1C**). The same animals were characterized by a significant reduction in spontaneous nocturnal food intake (**Fig. 1D, D^1**). However, the overall caloric intake [standard diet (SD) + palatable food (PF)] remained similar to controls, thus indicating a conserved maintenance in calories consumption despite reward-driven food intake (**Fig. 1E**). Importantly, isocaloric feeding was associated with conserved body weight (BW) and body composition (**Fig. 1F, Suppl. Fig. 1A, B**). A similar pattern of food reward-driven adaptations was also observed in female mice (**Suppl. Fig. 1C-E**).

Next, we investigated the consequences of BE on metabolic efficiency. Indirect calorimetry analysis revealed an increase in the respiratory exchange ratio (RER) before and after intermittent palatable food consumption (**Fig. 1G, G^1**), whilst a stark reduction was detected in the dark phase (**Fig. 1G**), thereby highlighting a metabolic shift of energy substrates use (from carbohydrates to lipids as indicated by RER ~1 or RER ~0.7, respectively). This was further confirmed by the modulation of fatty acid

oxidation (FAO, **Suppl. Fig. 1F**). In addition, we also observed an increased energy expenditure (EE) during the food anticipatory and consummatory phases (**Fig. 1H, H[1]**). Furthermore, infrared thermographic analysis revealed that BE was associated with a transient increase in brown adipose tissue (BAT) energy dissipation (**Fig. 1I**), while telemetric recording of core body temperature revealed a BE-specific increase during the anticipatory, consummatory and post-prandial phases (**Fig. 1J, J[1], Suppl. Fig. 1G**) and a sharp reduction during the last hours of the dark phase. Overall, changes in core body temperature were fostered around the time of locked palatable food access and overlapped with the increase in locomotor activity (**Fig. 1J, K**).

Access to calories-rich food and time-restricted feeding are invariably associated with changes in circulating signals reflecting metabolic and behavioral adaptations [25]. In line with this, we observed that our BE model was associated with reduced circulating triglycerides and insulin, and increased circulating corticosterone during the anticipatory phase (**Suppl. Fig. 1H-J**) while insulin sensitivity, as assessed by oral glucose tolerance test, remained unchanged (**Suppl. Fig. 1K, L**). These data indicate that homeostatic adaptations occurring during time-locked palatable feeding lead to changes in lipid-substrates utilization and promote adaptive activation of the hypothalamic-pituitary-adrenal (HPA) axis. However, bingeing did not elicit major changes in the expression of key hunger- and satiety-related hypothalamic genes (*Npy*, *Agrp*, *Pomc*, *Cart*, *Hcrt*, **Suppl. Fig. 1M**).

Overall, these results point to rapid reward-driven allostatic adaptations during which animals optimize their palatable food consumption and physiologically adapt, at the cost of regular chow food intake, to maintain a stable body weight.

BE induces dopamine-related modifications in a D1R-dependent manner

Dopamine (DA)-neurons and DA-sensitive structures, such as the dorsal striatum (DS) and the nucleus accumbens (NAc), are critical players in reward-based paradigms and in BE disorders [26, 27]. Here, we investigated whether and how bingeing modulated the DA-associated signaling machinery. The activations (phosphorylation) of the ribosomal protein S6 and the extracellular signal-regulated kinases (ERK) were used as functional readouts of DA-dependent molecular activity [28, 29] (**Suppl. Fig. 2A, B**). The food anticipatory phase was associated with an increase in phospho-ERK only in the DS (**Fig. 2A, B, Suppl. Fig. 2C**), mostly reflecting the increased locomotor activity during the anticipatory phase. Palatable

food consumption induced an increase in phospho-ERK and phospho-S6 (at both Ser$^{235/236}$ and Ser$^{240/244}$ sites) in both DS and NAc (**Fig. 2A, B, Suppl. Fig. 2C**). Interestingly, acute (single) consumption of palatable diet failed to trigger ERK and S6 activation (**Fig. 2A, B, Suppl. Fig. 2C**), revealing that molecular adaptations of DA signaling in the DS/NAc require the full establishment of BE and not only palatable food consumption. Immunofluorescence analysis further confirmed BE-induced S6 activation (**Suppl. Fig. 2D, E**).

Next, we wondered whether food-reward anticipatory and/or consummatory phases were followed by adaptive changes in DA signaling. We treated mice with GBR12909 (10 mg/kg), a specific DA transporter (DAT) blocker that leads to synaptic accumulation of DA. Interestingly, we observed a different behavior depending on BE phases (anticipatory *vs* consummatory). Before palatable food access, GBR similarly increased locomotor activity in both bingeing and control animals (**Fig. 2C, C^1**). However, when GBR was administered following palatable food consumption (1h), GBR-induced locomotor response was blunted in bingeing animals (**Fig. 2D, D^1**). These results indicate that BE-induced physiological adaptations are characterized by the enabled ability for palatable food to impinge on DA release and action.

At the postsynaptic level, DA acts onto medium spiny neurons (MSNs) which express either the dopamine D1R or D2R. In order to discriminate the role of D1R *vs* D2R signaling in BE, we pretreated animals with the D1R antagonist SCH23390 (0.1 mg/kg) or vehicle (Veh) 30 min prior access to palatable diet. SCH23390 dramatically reduced palatable food consumption (**Fig. 2E**). On the contrary, 30 min pretreatment with the D2R antagonist haloperidol (0.25 and 0.5 mg/kg) did not dampen palatable food consumption (**Fig. 2F**), even at cataleptic doses [30]. In line with this evidence, activation of striatal D1R leads to downstream phosphorylation of S6 and ERK [28, 29]. The adaptive molecular changes also required D1R activation since SCH23990 (0.1 mg/kg) largely suppressed BE-associated phosphorylation of S6 in both DS (**Fig. 2G, G^1, H^1**) and NAc (**Fig. 2G^2, H^2, Suppl. Fig. 2F**). Of note, although SCH23390 reduced binge-elicited anticipatory locomotor activity, basal locomotor activity in naive animals was not impaired (**Fig. 2I, I^1**), thereby excluding the confounding effects due to changes in basal locomotor activity. Furthermore, a compensatory rescue in chow intake was observed in SCH23390-pretreated bingeing animals during the dark phase, excluding potential long-lasting effects of the D1R inhibition (**Fig. 2J**). To further validate the implication of D1R in BE-elicited DA modifications,

we measured the locomotor activity triggered by the D1R agonist SKF81297 (5 mg/kg) at the end of the BE session (1h after food access). Interestingly, we observed an earlier (first 30 min) significant increase in locomotor activity in bingeing animals compared to control mice, although no major differences were detected during the cumulative 2-hrs response (**Fig. 2K, K[1]**).

Overall, our results reveal that the critical phases surrounding palatable food consumption in the context of BE profoundly affect D1R-associated signaling.

Peripheral endocannabinoids govern binge eating

Recent studies have highlighted the role of neuronal and endocrine gut systems in the regulation of food reward-seeking and DA-associated behaviors [31, 32]. We therefore tested whether gut-born metabolic signals had a privileged action onto BE-like consumption of palatable diet when compared to other known circulating satiety signals.

First, we observed that peripherally injected leptin (repeated 0.25 mg/kg, **Suppl. Fig. 3A, B**) or insulin (acute, 0.5 U/kg) did not trigger any reduction in palatable food consumption when administered in bingeing animals (**Fig. 3A**). Then, we investigated whether gut-born satiety signals retained anorectic properties with a similar protocol. GLP-1R agonists, exendin-4 (10 µg/kg) and liraglutide (100 µg/kg), successfully reduced binge-consumption of palatable diet (**Fig. 3A**). Moreover, pharmacological activation of GLP-1R, which did not alter spontaneous ambulatory activity, was also associated with a decrease in the anticipatory and consummatory locomotor phases (**Suppl. Fig. 3C, D**). Similarly, the cholecystokinin (CCK) analog CCK-8S (10 µg/kg) acutely decreased palatable food intake (**Fig. 3A**). Since only the anorectic action of gut-born signals was efficient in counteracting binge-like consumption, we also investigated the effect of endocannabinoids (eCBs) which are important signals in relaying nutrients-induced adaptive responses in the gut-brain axis [33, 34]. We acutely inhibited the CB1R with the global acting antagonist/inverse agonist AM251 (3 mg/kg, i.p.) and observed a dramatic reduction of BE-like consumption (**Fig. 3A**). Next, we wondered whether bingeing was accompanied by alterations in circulating peripheral eCBs [anandamide (AEA) and 2-arachidonoylglycerol (2-AG)] and eCBs-related species [docosahexanoyl ethanolamide (DHEA), oleoylethanolamide (OEA)]. While circulating *N*-acylethanolamines (AEA, DHEA, OEA) remained unaffected, bingeing induced a significant increase in circulating 2-AG (**Fig. 3B**). No differences

in central 2-AG levels were detected in key brain regions such as the hypothalamus, VTA, DS and NAc (**Suppl. Fig. 4A-D**).

Given the rise in peripheral 2-AG, we were eager to explore the role of peripheral CB1R signaling in BE outputs. Thus, we used the *bona fide* peripherally restricted CB1R neutral antagonist AM6545 (10 mg/kg, i.p.) or inverse agonist JD-5037 (3 mg/kg, i.p.), two compounds with poor blood brain barrier permeability [35–37]. Pretreatment (1h before bingeing) with AM6545 or JD-5037 induced a stark reduction of BE consumption when administered acutely (**Fig. 3C**). Conversely, the increase of 2-AG, achieved through the pharmacological inhibition (JZL184, 8 mg/kg) of its catabolic enzyme monoacylglycerol lipase (MAGL) [38], resulted in an increase of palatable food consumption that was fully prevented by AM6545 (**Fig. 3D**). This bidirectional modulatory action of eCBs/CB1R on BE did not show signs of desensitization and remained efficient throughout 4 days of daily pharmacological intervention (**Fig. 3E**). In the same line, thermogenic and locomotor activity analyses revealed that acute pretreatment with AM6545 strongly dampened both the anticipatory and consummatory phases of BE (**Fig. 3F, Suppl. Fig. 4E**) as well as the activation of S6 and cFos in the DS and NAc of bingeing mice (**Fig. 3G**) with no sex-dependent differences (**Suppl. Fig. 4F**). These results indicate that peripheral CB1R signaling is sufficient to control compulsive eating in BE and its reward-like molecular adaptations.

We next explored how peripheral CB1R signaling modulates metabolic efficiency in the context of BE. Pretreatment with AM6545 significantly increased fatty acid oxidation (FAO) (**Fig. 3H, H^{1}**). Importantly, this AM6545-induced FAO did not depend on reduced calorie intake (Binge session) or basal calorie contents (NoBinge session) (**Fig. 3H^{2}**) nor on altered energy expenditure (EE) (**Suppl. Fig. 4G**). These results indicate that acute manipulation of peripheral eCB tone affects nutrient partitioning and promotes a shift towards whole body lipid-substrate utilization. Importantly, oral administration (p.o.) of AM6545 did not blunt bingeing responses (**Fig. 3I**) nor increase FAO (**Fig. 3J**). These results suggest that, in our behavioral model, CB1R-mediated homeostatic adaptations do not depend on the lumen-oriented apical CB1R of endothelial or enteroendocrine intestinal cells [39, 40] but rather on non-lumen-oriented CB1R.

Given these results, we investigated the anatomo-functional structures at the interface between peripheral and central systems. Compared to control and bingeing mice, AM6545-pretreated bingeing mice showed a more pronounced neuronal activation in the caudal nucleus tractus solitarius (cNTS) and the area postrema (AP) (**Fig. 3K**) as well as in the cNTS-projecting lateral parabrachial nucleus (lPBN) (**Fig. 3L**), thus pointing the gut-brain vagal axis as potential mediator of our effects.

The gut-brain vagal axis is required for eCBs-mediated effects

Recent reports have indicated that CB1R is densely expressed in vagal afferent neurons [41]. To discriminate between all vagal afferents, we performed a meta-analysis on recent single-cell transcriptomic results [9] obtained through a path-specific viral strategy of gut segments (**Fig. 4A**). This analysis revealed that *Cnr1* (gene encoding for CB1R), but not *Cnr2*, is highly enriched in all segments of the gut-brain vagal axis (**Fig. 4B, Suppl. Fig. 4H, I**) and that, together with well-known afferent markers (*Slc17a6*, *Scn10a*, *Htr3a*, *Cartpt*, *Grin1*, *Phox2b*), *Cnr1* may be considered as a constitutive marker of vagal sensory neurons. Thus, we took advantage of subdiaphragmatic vagotomy (VGX) to investigate whether the eCBs-vagus axis was necessary/sufficient to mediate the modulatory effects of eCBs on BE.

First, we tested whether the pro-bingeing effects of the MAGL inhibitor JZL184 (**Fig. 3D, E**) required an intact vagal transmission. Although vagotomy *per se* was associated with a decrease in time-locked hedonic feeding (see **Fig. 4C, E**) and consequent BE-derived compensatory homeostatic adaptations (**Suppl. Fig. 5**), repeated inhibition (4 days) of MAGL (JZL184, 8 mg/kg) induced a significant increase of palatable food consumption only in sham animals (**Fig. 4C**).

Second, we tested whether the anti-bingeing effects of AM6545 were also routed by the vagus nerve. In sham mice, acute AM6545 led to a strong increase of cFos-positive neurons in the cNTS, AP and cNTS-projecting lPBN, while the signal was abolished in VGX mice (**Fig. 4D, D^1, D^2**). Of note, blockade of peripheral CB1R did not activate the rostral NTS (rNTS) (**Suppl. Fig. 4J**), thus indicating and further confirming that gut-to-brain vagal inputs are necessary to mediate the action of AM6545.

We also observed that the integrity of the vagus nerve was essential to mediate the anorectic action of AM6545 on BE behavior since the peripheral CB1R antagonist did

not trigger anti-bingeing responses in VGX mice compared to sham mice (**Fig. 4E**). Furthermore, vagotomy abolished the increase in FAO following AM6545 administration observed in sham mice (**Fig. 4F, F^1**, **G, G^1**), indicating that the gut-brain vagal communication routes feeding and the metabolic components associated with BE.

These vagus-dependent homeostatic adaptations promoted by the peripheral blockade of CB1R prompted us to investigate whether AM6545 was able to alter the activity of brainstem-projecting hypothalamic structures that control feeding. Indeed, AM6545 induced a strong vagus-dependent increase of cFos-positive neurons in the PVN and DMH regions (**Fig. 4H, I**), indicating that the metabolic adaptations induced by peripheral blockade of CB1R require a vagus-mediated cNTS→PBN→hypothalamus circuit whose nodes' activation control feeding and energy homeostasis [42–44].

Peripheral CB1R signaling routed by the vagus nerve controls the activity of VTA dopamine neurons

Palatable bingeing also strongly relies on central DA-dependent mechanisms (**Fig. 2**). Therefore, we explored the functional connection between peripheral eCBs and the gut-to-brain vagal axis in the modulation of the DA system. Since hedonic/motivated spontaneous feeding is blunted in AM6545-treated mice (**Fig. 3, 4**), a feature limiting further *in vivo* investigations of DA/reward events, we promoted and gauged the activity of the DA system by using pharmacological tools. Naive mice were acutely pretreated with AM6545 (or JD-5037) or vehicle 1h before being administered with the DAT blocker GBR12909. Blockade of peripheral CB1R drastically reduced GBR-induced locomotor activity (**Fig. 5A, A^1, B, B^1**) as well as GBR-triggered cFos in the striatum (**Fig. 5C, C^1**). To further study *in vivo* DA dynamics, we took advantage of the virally expressed DA biosensor dLight1.2 coupled to *in vivo* fiber photometry [22]. Importantly, pretreatment with AM6545 blunted GBR-evoked accumbal DA accumulation (**Fig. 5D, D^1**). Interestingly, unlike the brain penetrant CB1R antagonist/inverse agonist AM251, the peripheral AM6545 failed in counteracting amphetamine-induced locomotor activity (**Fig. 5E, F, Suppl. Fig. 6A**). This evidence indicates a clear difference in the action of peripheral *vs* central CB1R and suggests that inhibition of peripheral CB1R may modulate the

intrinsic spontaneous activity of DA-neurons rather than altering evoked DA release events.

Altogether, these results reveal that inhibition of peripheral CB1R, besides promoting satiety and FAO (**Fig. 3, 4**), may dampen reward-driven feeding also by concomitantly reducing DA-neurons spontaneous activity and consequent activation of dopaminoceptive structures.

To directly address this point, VGX mice were acutely pretreated with AM6545 1h prior GBR12909. Remarkably, ablation of the vagus nerve abolished the blunting effect of AM6545 on GBR-elicited locomotor activity (**Fig. 5G, G[1]**). Moreover, consistently with what observed for palatable bingeing (**Fig. 3I**), this vagus-to-brain effect was further highlighted by the lack of action of AM6545 when orally administered (**Fig. 5H, Suppl. Fig. 6B**).

Finally, to fully establish that peripheral inhibition of CB1R modulates the activity of VTA DA-neurons, we performed cell type-specific *in vivo* Ca^{2+} imaging of DA-neurons in presence or absence of AM6545. We took advantage of *Drd2*-Cre mice to virally express GCaMP6f in VTA DA-neurons (**Fig. 6A**) as they co-express the autoreceptor D2R (**Suppl. Fig. 6C**). Indeed, using this mouse line we were able to detect activation and inhibition of VTA DA-neurons following rewarding (high-fat high-sugar pellet) or aversive (scruff restraint) events (**Suppl. Fig. 6D, E**), respectively. To trigger the activity of DA-neurons independently from food- or drugs-associated stimuli, we used two paradigms that modulate DA-neurons: the tail suspension [45] and exposure to a new environment [46] which promotes exploration (**Fig. 6B**). Inhibition of peripheral CB1R led to a reduced activation of VTA DA-neurons during both paradigms (**Fig. 6C, D**). At the behavioral level, while AM6545 did not alter the time of immobility in the tail suspension test (**Fig. 6E**), it reduced the exploratory drive in a vagus-dependent manner (**Fig. 6F, F[1]**). Of note, the brain permeable AM251 reduced exploratory drive in a vagus-independent manner (**Fig. 6G**).

Collectively, these results reveal that peripheral CB1R signaling routed through the vagal axis exerts an integrative control over metabolic/satietogenic (**Fig. 3, 4**) and DA paths (**Fig. 5, 6**), both of which are pivotal for the establishment of BE.

Discussion

A characteristic feature of feeding behavior is its key ability to dynamically adapt to sensory and environmental stimuli signaling food availability. Such adaptive strategy is even more pronounced when food is palatable and energy-dense. Indeed, the control of feeding strategies requires complex and highly interactive systems that can hardly be unequivocally attributed to single structures, circuits or mediators.

In our study, we observed that, first, palatable time-locked feeding mobilizes both homeostatic and hedonic components of feeding through fast, but yet physiological, allostatic adaptations. Second, such allostatic adaptations require a concerted involvement of central DA (hedonic drive) and peripheral eCBs signaling (homeostatic and hedonic drive). Third, the permissive role of peripheral eCBs fully relies on the vagus nerve which, by a polysynaptic circuit, controls the activity of both satietogenic and reward (dopamine) structures. Fourth, our results point to peripheral CB1R neutral antagonists as promising therapeutic tools to counteract eating as well as reward-related disorders.

Overall, our study describes for the first time the fundamental role of eCB gut-brain transmission as a core component of binge eating and its behavioral, cellular and molecular adaptations.

Here, by investigating the pathways involved in hedonic feeding in absence of hunger or energy deprivation, we provide evidence that the hedonic drive to eat, as triggered by our intermittent time-locked model, promotes rapid homeostatic compensations leading to escalating consumption of palatable food and to allostatic adaptations of energy metabolism. As such, caloric demands are fulfilled and classical energy-mediated homeostatic signals (leptin, insulin) do not seem to spontaneously interfere, thus providing us the opportunity to study food intake-related integrative pathways with the abstraction of the homeostatic *vs* hedonic discrepancy. In line with clinical data [47, 48], we observed that binge-like feeding in lean animals is not necessarily associated with overweight gain. The allostatic adaptations observed, ranging from increased anticipatory feeding phase to pre-feeding increased corticosterone levels and food intake maximization, all represent key hallmarks of the compulsive and emotional states of BE patients [49–51]. The anticipatory feeding phase was associated with decreased levels of plasma TG and

insulin, whereas both anticipatory and consummatory phases were characterized by increased energy expenditure, core temperature and metabolic efficiency, thereby suggesting a metabolic shift of nutrients' use. This observation perfectly mirrors the allostatic theory, which stands on the fact that an organism anticipates and adapts to environmental changes while accordingly adjusting several physiological parameters to maintain stable physiological states [52, 53]. Allostatic mechanisms have classically been discussed in terms of stress-related regulatory events. However, the hedonic value of a stimulus (food, recreational drugs) can function as a feed-forward allostatic factor [4].

In line with this notion, analysis of key DA-activated downstream targets in the DS and NAc highlighted specific patterns of molecular activation. Notably, while the anticipatory phase was associated with an increase in ERK and $S6^{Ser235/236}$ phosphorylations, the consummatory phase was also accompanied by a robust increase in mTOR-mediated $S6^{Ser240/244}$ activation. Such signaling events, which did not depend on a single episode of palatable food intake, required the dopamine D1R. Whether this molecular regulation reflects the full establishment of BE or the amount of ingested palatable food remains to be established. Nevertheless, this D1R mechanism is of interest since, contrary to the well-known molecular insights of drugs of abuse also requiring the D1R [54–56], food-related disorders have usually been predominantly associated with altered D2R signaling [57, 58]. Our results reveal that binge eating, characterized by transients and sudden urges of hedonic drive, requires, at least in its early phases, a D1R-mediated transmission. This D1R-dependent mechanism is in line with the affinity and time-dependent dynamics of dopamine effects [54] as well as with the molecular action of released DA which, by binding to $G\alpha$(olf)-coupled D1R, would trigger the activation of the aforementioned pathways, while activation of the Gi-coupled D2R would lead to their inhibition. However, in clear opposition to psychostimulants, which directly act at central DA synapses, food and food-mediated behaviors impact on DA transmission through a plethora of indirect and often peripherally born long-range acting mediators. Notably, nutrients, as demonstrated by intragastric infusion of fat and sugar [14, 59–61], or gut-born signals [62–64], are sufficient to modulate DA release in reward-related structures. Here, we observed that gut-born signals such as CCK, GLP1 and endocannabinoids (eCBs) are essential in gating bingeing. In particular, we found

that time-locked consumption of palatable food was associated with a rise in peripheral endogenous eCBs, notably 2-AG. Furthermore, inhibition of the 2-AG-degrading enzyme MAG lipase resulted in a potentiation of palatable food consumption. Thus, by taking advantage of low brain permeant CB1R antagonists/inverse agonists, we observed that blockade of CB1R was able to fully abolish both anticipatory and consummatory phases of hedonic feeding as well as the potentiated feeding induced by the MAG lipase inhibitor. These effects agree with the literature showing that endogenous peripheral eCBs are highly and dynamically modulated in eating disorders, and act as powerful mediators of the gut-to-brain integration [17].

Previous studies have shown that (chronic) administration of AM6545 promoted long-term maintenance of weight loss and reduction of dyslipidemia in obesity [35, 37]. Here, we show that a single, as well as repeated (4 days), administration of AM6545 potently inhibits binge eating and its molecular adaptations. The anorectic effects of peripheral blockade of CB1R have been, at least in part, attributed to the property of global CB1R antagonists to promote fatty acid oxidation (FAO). In agreement with these studies, we have observed that acute administration of AM6545 was able to dramatically increase FAO independently of food intake. However, here we also demonstrate that such effects require the vagus nerve. The action of endogenous eCBs as well as of AM6545 on CB1R-expressing vagal afferents [41] may explain our results. In fact, an increase in endogenous eCBs during palatable feeding would slow the vagus nerve activity through the inhibitory Gi-coupled signaling of CB1R, thus delaying cNTS-reaching satiety signals and promoting food intake. On the contrary, peripheral blockade of CB1R, especially when peripheral eCB levels are endogenously high (*i.e.* binge eating, bulimia, obesity), would lead to a prompt disinhibition and to the concomitant activation of satietogenic brain pathways (cNTS→PBN→PVN). Moreover, it is worth to mention that under fasting or lipoprivic conditions the systemic CB1R inverse agonist SR141716A modulated feeding by the vagal and sympathetic systems [65]. Another site of action for peripheral eCBs is represented by CB1R-expressing gut cells [40, 66]. Interestingly, oral administration of a peripheral CB1R antagonist resulted in a reduction of alcohol intake via a ghrelin-dependent and vagus-mediated mechanism [66]. However, in our reward-driven feeding model, oral administration of AM6545

failed to modulate metabolic efficiency as well as to prevent bingeing behavior, thus suggesting that lumen-oriented apical CB1R may not be involved in our mechanism. Intriguingly, recent studies have uncovered that sensory neuropod cells in the gut [67] can synaptically signal with the juxtaposed vagal afferents using, among other possible mediators [68], the fast-acting neurotransmitter glutamate [10]. Whether this specialized gut-to-nerve synapse also mobilizes eCBs, as it occurs at most central excitatory synapses, remains to be determined. In addition, it is important to highlight the key role of peripheral CB1R in adipocytes in the regulation of energy balance [69]. However, whether and how adipocytes may, indeed indirectly, influence the vagal axis is yet unclear.

Overall, it would not be hazardous to suggest that peripheral eCBs may impact feeding patterns through different integrative mechanisms which, depending on the location of peripheral CB1R, may strongly modulate distinct hedonic and homeostatic functional outputs. These results call for cell-type and tissue-type-specific strategies to selectively delete CB1R and/or eCBs-producing enzymes in distinct compartments of the gastrointestinal tract and in the neuronal gut-brain axis.

To anatomically provide an explanatory gut-to-brain circuit able to support the vagus-mediated action of AM6545, we found a stark increase of cFos, a marker of neuronal activity, in key brain regions of the satietogenic neuronal pathway. Importantly, we reveal that blockade of peripheral CB1R signaling resulted in a strong vagus-dependent activation of the cNTS as well as of its downstream projecting structures, notably the lPBN and the hypothalamic PVN. This segmented activation of the gut→brainstem→hypothalamus path is most likely responsible for the AM6545-induced effects on bingeing and energy homeostasis since structure-specific activation of these nodes has been shown to reduce food intake and alters energy homeostasis [43, 70–72]. In addition to this satietogenic path and given the strong reward component of our paradigm, we also uncover that AM6545-mediated vagus activation results in a dampened activation of VTA DA-neurons. However, such effect did not depend on the releasing capabilities of DA-neurons since AM6545 failed to alter amphetamine-evoked locomotor activity. In addition, taking advantage of virally mediated GCaMP6f-mediated *in vivo* Ca^{2+} imaging of putative VTA DA-neurons, here we demonstrate that peripheral blockade of CB1R clearly reduced both basal and evoked activity of DA-neurons, a feature resembling some neurochemical effects of vagal nerve stimulation [73, 74].

The VTA is characterized by a highly heterogeneous connectivity [75], and a single and monosynaptic circuit responsible for the inhibition of DA-neurons through the AM6545-activated vagus nerve cannot be selectively sorted out yet. However, several satiety-related structures in the brainstem and hypothalamus are known to project and modulate, directly and/or indirectly, VTA DA-neurons [13, 76–79]. Among these circuits, the PBN→VTA relay is of particular interest since excitatory PBN neurons also largely contact VTA GABA-neurons [78, 80] which in turn may drive the inhibition of VTA DA-neurons and consequent dampening of motivated behaviors.

Here, we show that DA-dependent adaptations require orchestrated inputs among which peripheral endocannabinoids, through the vagus nerve, allostatically scale the homeostatic and hedonic components of feeding and act as mandatory gatekeepers for adaptive responses of the reward circuit. The gut-brain axis is increasingly incriminated as a key player of the regulation of energy metabolism [81], and we show for the first time that BE is under the control of the vagus-mediated peripheral inputs. Pointing to peripheral eCBs as permissive actors of this eating disorder certainly brings novelty to the clinical investigations aimed at identifying innovative and non-invasive therapeutic strategies. Importantly, this study further points to the gut-brain axis as a privileged target to modulate brain structures that are functionally responsible for processing cognitive and reward events in an integrative manner.

In conclusion, while further studies are warranted to fully untangle the key enteric actors responsible for this phenomenon, our study identifies a novel integrative mechanism by which peripheral endocannabinoids through the gut-brain vagal axis gate allostatic feeding by controlling satiety and reward events, thus also paving the way to target peripheral elements for brain disorders.

Acknowledgments

We thank Chloé Morel, Rim Hassouna, Anne-Sophie Delbes, Daniela Herrera Moro and Raphaël Denis for technical advice and support. Adrien Paquot (BPBL/UCLouvain) is acknowledged for his help with eCB quantification. We thank Olja Kacanski for administrative support, Isabelle Le Parco, Ludovic Maingault, Angélique Dauvin, Aurélie Djemat, Florianne Michel, Magguy Boa and Daniel Quintas for animals' care and Sabria Allithi for genotyping. We acknowledge the technical platform Functional and Physiological Exploration platform (FPE) of the Université de Paris (BFA-UMR 8251) and the animal core facility Buffon of the Université de Paris/Institut Jacques Monod. This work was supported by the Fyssen Foundation, Nutricia Research Foundation, Allen Foundation Inc., Université de Paris and CNRS. CB and EM were supported by fellowships from the *Fondation pour la Recherche Médicale* (FRM). Telemetry experiments were supported by the Continuous Glucose Telemetry Award 2018 (Dr. Denis) and sponsored by Data Sciences International.

Author Contributions

C.B. and G.G. conceived, designed, performed and analyzed most of the experiments. J.C. performed surgeries and behavioral experiments. E.M. helped with molecular studies. E.F. performed vagotomy. C.M. helped with fiber photometry experiments. G.G.M. and R.T. analyzed endocannabinoids levels. S.L. provided scientific guidance and critical feedback. G.G. supervised the whole project, interpreted the data and wrote the manuscript with contribution from all coauthors.

Competing interests

The authors declare no competing interests.

References

1. Berthoud H-R, Münzberg H, Morrison CD. Blaming the Brain for Obesity: Integration of Hedonic and Homeostatic Mechanisms. Gastroenterology. 2017;152:1728–1738.
2. Lenard NR, Berthoud H-R. Central and peripheral regulation of food intake and physical activity: pathways and genes. Obesity (Silver Spring). 2008;16 Suppl 3:S11-22.
3. McEwen BS, Wingfield JC. The concept of allostasis in biology and biomedicine. Horm Behav. 2003;43:2–15.
4. George O, Le Moal M, Koob GF. Allostasis and addiction: role of the dopamine and corticotropin-releasing factor systems. Physiol Behav. 2012;106:58–64.
5. Volkow ND, Wang G-J, Baler RD. Reward, dopamine and the control of food intake: implications for obesity. Trends Cogn Sci (Regul Ed). 2011;15:37–46.
6. Mazier W, Saucisse N, Simon V, Cannich A, Marsicano G, Massa F, et al. mTORC1 and CB1 receptor signaling regulate excitatory glutamatergic inputs onto the hypothalamic paraventricular nucleus in response to energy availability. Mol Metab. 2019;28:151–159.
7. Rossi MA, Basiri ML, McHenry JA, Kosyk O, Otis JM, van den Munkhof HE, et al. Obesity remodels activity and transcriptional state of a lateral hypothalamic brake on feeding. Science. 2019;364:1271–1274.
8. Beutler LR, Corpuz TV, Ahn JS, Kosar S, Song W, Chen Y, et al. Obesity causes selective and long-lasting desensitization of AgRP neurons to dietary fat. Elife. 2020;9.
9. Bai L, Mesgarzadeh S, Ramesh KS, Huey EL, Liu Y, Gray LA, et al. Genetic Identification of Vagal Sensory Neurons That Control Feeding. Cell. 2019;179:1129-1143.e23.
10. Kaelberer MM, Buchanan KL, Klein ME, Barth BB, Montoya MM, Shen X, et al. A gut-brain neural circuit for nutrient sensory transduction. Science. 2018;361.
11. de Lartigue G. Role of the vagus nerve in the development and treatment of diet-induced obesity. J Physiol. 2016;594:5791–5815.
12. Fernandes AB, Alves da Silva J, Almeida J, Cui G, Gerfen CR, Costa RM, et al. Postingestive Modulation of Food Seeking Depends on Vagus-Mediated Dopamine Neuron Activity. Neuron. 2020;106:778-788.e6.
13. Han W, Tellez LA, Perkins MH, Perez IO, Qu T, Ferreira J, et al. A Neural Circuit for Gut-Induced Reward. Cell. 2018;175:665-678.e23.
14. Hankir MK, Seyfried F, Hintschich CA, Diep T-A, Kleberg K, Kranz M, et al. Gastric Bypass Surgery Recruits a Gut PPAR-α-Striatal D1R Pathway to Reduce Fat Appetite in Obese Rats. Cell Metab. 2017;25:335–344.
15. Argueta DA, DiPatrizio NV. Peripheral endocannabinoid signaling controls hyperphagia in western diet-induced obesity. Physiol Behav. 2017;171:32–39.
16. DiPatrizio NV, Joslin A, Jung K-M, Piomelli D. Endocannabinoid signaling in the gut mediates preference for dietary unsaturated fats. FASEB J. 2013;27:2513–2520.
17. Gómez R, Navarro M, Ferrer B, Trigo JM, Bilbao A, Del Arco I, et al. A peripheral mechanism for CB1 cannabinoid receptor-dependent modulation of feeding. J Neurosci. 2002;22:9612–9617.
18. Monteleone P, Matias I, Martiadis V, De Petrocellis L, Maj M, Di Marzo V. Blood levels of the endocannabinoid anandamide are increased in anorexia nervosa and in binge-eating disorder, but not in bulimia nervosa. Neuropsychopharmacology.

2005;30:1216–1221.
19. Monteleone AM, Piscitelli F, Dalle Grave R, El Ghoch M, Di Marzo V, Maj M, et al. Peripheral Endocannabinoid Responses to Hedonic Eating in Binge-Eating Disorder. Nutrients. 2017;9.
20. Kuipers EN, Kantae V, Maarse BCE, van den Berg SM, van Eenige R, Nahon KJ, et al. High Fat Diet Increases Circulating Endocannabinoids Accompanied by Increased Synthesis Enzymes in Adipose Tissue. Front Physiol. 2018;9:1913.
21. Berland C, Montalban E, Perrin E, Di Miceli M, Nakamura Y, Martinat M, et al. Circulating Triglycerides Gate Dopamine-Associated Behaviors through DRD2-Expressing Neurons. Cell Metab. 2020;31:773-790.e11.
22. Patriarchi T, Cho JR, Merten K, Howe MW, Marley A, Xiong W-H, et al. Ultrafast neuronal imaging of dopamine dynamics with designed genetically encoded sensors. Science. 2018;360.
23. Avena NM. The study of food addiction using animal models of binge eating. Appetite. 2010;55:734–737.
24. DiFeliceantonio AG, Coppin G, Rigoux L, Edwin Thanarajah S, Dagher A, Tittgemeyer M, et al. Supra-Additive Effects of Combining Fat and Carbohydrate on Food Reward. Cell Metab. 2018;28:33-44.e3.
25. Oosterman JE, Koekkoek LL, Foppen E, Unmehopa UA, Eggels L, Verheij J, et al. Synergistic Effect of Feeding Time and Diet on Hepatic Steatosis and Gene Expression in Male Wistar Rats. Obesity (Silver Spring). 2020;28 Suppl 1:S81–S92.
26. Wang G-J, Geliebter A, Volkow ND, Telang FW, Logan J, Jayne MC, et al. Enhanced striatal dopamine release during food stimulation in binge eating disorder. Obesity (Silver Spring). 2011;19:1601–1608.
27. Spierling S, de Guglielmo G, Kirson D, Kreisler A, Roberto M, George O, et al. Insula to ventral striatal projections mediate compulsive eating produced by intermittent access to palatable food. Neuropsychopharmacology. 2020;45:579–588.
28. Biever A, Puighermanal E, Nishi A, David A, Panciatici C, Longueville S, et al. PKA-dependent phosphorylation of ribosomal protein S6 does not correlate with translation efficiency in striatonigral and striatopallidal medium-sized spiny neurons. J Neurosci. 2015;35:4113–4130.
29. Gangarossa G, Perroy J, Valjent E. Combinatorial topography and cell-type specific regulation of the ERK pathway by dopaminergic agonists in the mouse striatum. Brain Struct Funct. 2013;218:405–419.
30. Radl D, Chiacchiaretta M, Lewis RG, Brami-Cherrier K, Arcuri L, Borrelli E. Differential regulation of striatal motor behavior and related cellular responses by dopamine D2L and D2S isoforms. Proc Natl Acad Sci U S A. 2018;115:198–203.
31. Reichelt AC, Westbrook RF, Morris MJ. Integration of reward signalling and appetite regulating peptide systems in the control of food-cue responses. Br J Pharmacol. 2015;172:5225–5238.
32. de Araujo IE, Schatzker M, Small DM. Rethinking Food Reward. Annual Review of Psychology. 2020;71:139–164.
33. DiPatrizio NV, Piomelli D. Intestinal lipid-derived signals that sense dietary fat. J Clin Invest. 2015;125:891–898.
34. Lau BK, Cota D, Cristino L, Borgland SL. Endocannabinoid modulation of homeostatic and non-homeostatic feeding circuits. Neuropharmacology. 2017;124:38–51.
35. Cluny NL, Vemuri VK, Chambers AP, Limebeer CL, Bedard H, Wood JT, et al. A novel peripherally restricted cannabinoid receptor antagonist, AM6545, reduces food intake and body weight, but does not cause malaise, in rodents. Br J

Pharmacol. 2010;161:629–642.
36. Tam J, Cinar R, Liu J, Godlewski G, Wesley D, Jourdan T, et al. Peripheral cannabinoid-1 receptor inverse agonism reduces obesity by reversing leptin resistance. Cell Metab. 2012;16:167–179.
37. Tam J, Vemuri VK, Liu J, Bátkai S, Mukhopadhyay B, Godlewski G, et al. Peripheral CB1 cannabinoid receptor blockade improves cardiometabolic risk in mouse models of obesity. J Clin Invest. 2010;120:2953–2966.
38. Long JZ, Li W, Booker L, Burston JJ, Kinsey SG, Schlosburg JE, et al. Selective blockade of 2-arachidonoylglycerol hydrolysis produces cannabinoid behavioral effects. Nat Chem Biol. 2009;5:37–44.
39. Sykaras AG, Demenis C, Case RM, McLaughlin JT, Smith CP. Duodenal enteroendocrine I-cells contain mRNA transcripts encoding key endocannabinoid and fatty acid receptors. PLoS One. 2012;7:e42373.
40. Argueta DA, Perez PA, Makriyannis A, DiPatrizio NV. Cannabinoid CB1 Receptors Inhibit Gut-Brain Satiation Signaling in Diet-Induced Obesity. Front Physiol. 2019;10:704.
41. Egerod KL, Petersen N, Timshel PN, Rekling JC, Wang Y, Liu Q, et al. Profiling of G protein-coupled receptors in vagal afferents reveals novel gut-to-brain sensing mechanisms. Mol Metab. 2018;12:62–75.
42. Grill HJ, Hayes MR. Hindbrain neurons as an essential hub in the neuroanatomically distributed control of energy balance. Cell Metab. 2012;16:296–309.
43. D'Agostino G, Lyons DJ, Cristiano C, Burke LK, Madara JC, Campbell JN, et al. Appetite controlled by a cholecystokinin nucleus of the solitary tract to hypothalamus neurocircuit. Elife. 2016;5.
44. Cheng W, Gonzalez I, Pan W, Tsang AH, Adams J, Ndoka E, et al. Calcitonin Receptor Neurons in the Mouse Nucleus Tractus Solitarius Control Energy Balance via the Non-aversive Suppression of Feeding. Cell Metab. 2020;31:301-312.e5.
45. Kolata SM, Nakao K, Jeevakumar V, Farmer-Alroth EL, Fujita Y, Bartley AF, et al. Neuropsychiatric Phenotypes Produced by GABA Reduction in Mouse Cortex and Hippocampus. Neuropsychopharmacology. 2018;43:1445–1456.
46. Takeuchi T, Duszkiewicz AJ, Sonneborn A, Spooner PA, Yamasaki M, Watanabe M, et al. Locus coeruleus and dopaminergic consolidation of everyday memory. Nature. 2016;537:357–362.
47. Hutson PH, Balodis IM, Potenza MN. Binge-eating disorder: Clinical and therapeutic advances. Pharmacol Ther. 2018;182:15–27.
48. Carr MM, Grilo CM. Examining heterogeneity of binge-eating disorder using latent class analysis. J Psychiatr Res. 2020;130:194–200.
49. Naish KR, Laliberte M, MacKillop J, Balodis IM. Systematic review of the effects of acute stress in binge eating disorder. Eur J Neurosci. 2019;50:2415–2429.
50. Bake T, Murphy M, Morgan DGA, Mercer JG. Large, binge-type meals of high fat diet change feeding behaviour and entrain food anticipatory activity in mice. Appetite. 2014;77:60–71.
51. Muñoz-Escobar G, Guerrero-Vargas NN, Escobar C. Random access to palatable food stimulates similar addiction-like responses as a fixed schedule, but only a fixed schedule elicits anticipatory activation. Sci Rep. 2019;9:18223.
52. Ramsay DS, Woods SC. Clarifying the roles of homeostasis and allostasis in physiological regulation. Psychol Rev. 2014;121:225–247.
53. De Ridder D, Manning P, Leong SL, Ross S, Vanneste S. Allostasis in health and food addiction. Sci Rep. 2016;6:37126.

54. Luo Z, Volkow ND, Heintz N, Pan Y, Du C. Acute cocaine induces fast activation of D1 receptor and progressive deactivation of D2 receptor striatal neurons: in vivo optical microprobe [Ca2+]i imaging. J Neurosci. 2011;31:13180–13190.
55. Kai N, Nishizawa K, Tsutsui Y, Ueda S, Kobayashi K. Differential roles of dopamine D1 and D2 receptor-containing neurons of the nucleus accumbens shell in behavioral sensitization. J Neurochem. 2015;135:1232–1241.
56. Bertran-Gonzalez J, Bosch C, Maroteaux M, Matamales M, Hervé D, Valjent E, et al. Opposing patterns of signaling activation in dopamine D1 and D2 receptor-expressing striatal neurons in response to cocaine and haloperidol. J Neurosci. 2008;28:5671–5685.
57. Kenny PJ, Voren G, Johnson PM. Dopamine D2 receptors and striatopallidal transmission in addiction and obesity. Curr Opin Neurobiol. 2013;23:535–538.
58. Caravaggio F, Raitsin S, Gerretsen P, Nakajima S, Wilson A, Graff-Guerrero A. Ventral striatum binding of a dopamine D2/3 receptor agonist but not antagonist predicts normal body mass index. Biol Psychiatry. 2015;77:196–202.
59. Han W, Tellez LA, Niu J, Medina S, Ferreira TL, Zhang X, et al. Striatal Dopamine Links Gastrointestinal Rerouting to Altered Sweet Appetite. Cell Metab. 2016;23:103–112.
60. Tellez LA, Han W, Zhang X, Ferreira TL, Perez IO, Shammah-Lagnado SJ, et al. Separate circuitries encode the hedonic and nutritional values of sugar. Nat Neurosci. 2016;19:465–470.
61. Alhadeff AL, Goldstein N, Park O, Klima ML, Vargas A, Betley JN. Natural and Drug Rewards Engage Distinct Pathways that Converge on Coordinated Hypothalamic and Reward Circuits. Neuron. 2019;103:891-908.e6.
62. Cone JJ, McCutcheon JE, Roitman MF. Ghrelin acts as an interface between physiological state and phasic dopamine signaling. J Neurosci. 2014;34:4905–4913.
63. Fulton S, Pissios P, Manchon RP, Stiles L, Frank L, Pothos EN, et al. Leptin regulation of the mesoaccumbens dopamine pathway. Neuron. 2006;51:811–822.
64. Reddy IA, Smith NK, Erreger K, Ghose D, Saunders C, Foster DJ, et al. Bile diversion, a bariatric surgery, and bile acid signaling reduce central cocaine reward. PLoS Biol. 2018;16:e2006682.
65. Bellocchio L, Soria-Gómez E, Quarta C, Metna-Laurent M, Cardinal P, Binder E, et al. Activation of the sympathetic nervous system mediates hypophagic and anxiety-like effects of CB_1 receptor blockade. Proc Natl Acad Sci U S A. 2013;110:4786–4791.
66. Godlewski G, Cinar R, Coffey NJ, Liu J, Jourdan T, Mukhopadhyay B, et al. Targeting Peripheral CB1 Receptors Reduces Ethanol Intake via a Gut-Brain Axis. Cell Metab. 2019;29:1320-1333.e8.
67. Bohórquez DV, Shahid RA, Erdmann A, Kreger AM, Wang Y, Calakos N, et al. Neuroepithelial circuit formed by innervation of sensory enteroendocrine cells. J Clin Invest. 2015;125:782–786.
68. Haber AL, Biton M, Rogel N, Herbst RH, Shekhar K, Smillie C, et al. A single-cell survey of the small intestinal epithelium. Nature. 2017;551:333–339.
69. Ruiz de Azua I, Mancini G, Srivastava RK, Rey AA, Cardinal P, Tedesco L, et al. Adipocyte cannabinoid receptor CB1 regulates energy homeostasis and alternatively activated macrophages. J Clin Invest. 2017;127:4148–4162.
70. Roman CW, Derkach VA, Palmiter RD. Genetically and functionally defined NTS to PBN brain circuits mediating anorexia. Nat Commun. 2016;7:11905.
71. Carter ME, Soden ME, Zweifel LS, Palmiter RD. Genetic identification of a

neural circuit that suppresses appetite. Nature. 2013;503:111–114.
72. Li MM, Madara JC, Steger JS, Krashes MJ, Balthasar N, Campbell JN, et al. The Paraventricular Hypothalamus Regulates Satiety and Prevents Obesity via Two Genetically Distinct Circuits. Neuron. 2019;102:653-667.e6.
73. Manta S, El Mansari M, Debonnel G, Blier P. Electrophysiological and neurochemical effects of long-term vagus nerve stimulation on the rat monoaminergic systems. Int J Neuropsychopharmacol. 2013;16:459–470.
74. Perez SM, Carreno FR, Frazer A, Lodge DJ. Vagal nerve stimulation reverses aberrant dopamine system function in the methylazoxymethanol acetate rodent model of schizophrenia. J Neurosci. 2014;34:9261–9267.
75. Morales M, Margolis EB. Ventral tegmental area: cellular heterogeneity, connectivity and behaviour. Nat Rev Neurosci. 2017;18:73–85.
76. Alhadeff AL, Rupprecht LE, Hayes MR. GLP-1 neurons in the nucleus of the solitary tract project directly to the ventral tegmental area and nucleus accumbens to control for food intake. Endocrinology. 2012;153:647–658.
77. Nieh EH, Vander Weele CM, Matthews GA, Presbrey KN, Wichmann R, Leppla CA, et al. Inhibitory Input from the Lateral Hypothalamus to the Ventral Tegmental Area Disinhibits Dopamine Neurons and Promotes Behavioral Activation. Neuron. 2016;90:1286–1298.
78. Faget L, Osakada F, Duan J, Ressler R, Johnson AB, Proudfoot JA, et al. Afferent Inputs to Neurotransmitter-Defined Cell Types in the Ventral Tegmental Area. Cell Rep. 2016;15:2796–2808.
79. Wang X-F, Liu J-J, Xia J, Liu J, Mirabella V, Pang ZP. Endogenous Glucagon-like Peptide-1 Suppresses High-Fat Food Intake by Reducing Synaptic Drive onto Mesolimbic Dopamine Neurons. Cell Rep. 2015;12:726–733.
80. Beier KT, Steinberg EE, DeLoach KE, Xie S, Miyamichi K, Schwarz L, et al. Circuit Architecture of VTA Dopamine Neurons Revealed by Systematic Input-Output Mapping. Cell. 2015;162:622–634.
81. Clemmensen C, Müller TD, Woods SC, Berthoud H-R, Seeley RJ, Tschöp MH. Gut-Brain Cross-Talk in Metabolic Control. Cell. 2017;168:758–774.

Figure legends

Fig. 1: Allostatic adaptations of metabolic efficiency to time-locked access to palatable diet. (**A**) Experimental design. Control (Ctr) or bingeing animals (Binge) had daily intermittent access to water or a palatable lipids/sucrose mixture for 1 hour/day during 10-14 consecutive days. Regular chow pellets were provided *ad libitum* throughout the entire experiment. (**B**) Daily binge consumption (ml) of palatable mixture during a 14-days protocol. Statistics: ***p<0.001 Binge *vs* Control. (**C**) 24 hrs locomotor activity in calorimetric chambers (average of 3 consecutive days). Red dotted rectangles indicate the locomotor activity 2-hrs prior and after palatable food access. (**C^1**) Cumulative locomotor activity 2-hrs prior and after palatable food access. Results are expressed as beam breaks (bb). Statistics: *p<0.05 and ***p<0.001 Binge *vs* Control. (**D**) Temporal pattern of regular chow food intake (FI, kcal/h) during 24 hrs (average of 3 consecutive days). Statistics: **p<0.01 Binge *vs* Control. (**D^1**) Cumulative chow food intake during the dark period. Statistics: ***p<0.001 Binge *vs* Control. (**E**) 24 hrs food intake considering all calories: standard diet (SD) and palatable food (PF). Statistics: ***p<0.001 Binge(SD) *vs* Control(SD), $^{###}$p<0.001 Binge(SD+PF) *vs* Binge(SD). (**F**) Body weight throughout the 14-days experimental procedure. (**G**) Longitudinal profile of the respiratory energy ratio (RER) from indirect calorimetry (average of 3 consecutive days) and (**G^1**) averaged RER values 2-hrs prior and after palatable food access. Statistics: **p<0.01 and ***p<0.001 Binge *vs* Control. (**H**) Longitudinal profile of energy expenditure (EE) from indirect calorimetry (average of 3 consecutive days) and (**H^1**) averaged EE values 2-hrs prior and after palatable food access. Statistics: *p<0.05 and **p<0.01 Binge *vs* Control. (**I**) Brown adipose tissue (BAT) temperature during bingeing. Statistics: *p<0.05 and **p<0.01 Binge *vs* Control. (**J**) Real-time core temperature recording during 24 hrs and (**J^1**) averaged values 2-hrs prior and after palatable food access. Statistics: ***p<0.001 Binge *vs* Control. (**K**) Matching locomotor activity from core temperature measurements. Statistics: ***p<0.001 Binge *vs* Control. For number of mice/group and statistical details see **Suppl. Table 1**.

Fig. 2: Binge eating induces dopamine D1R-related molecular modifications. (**A, B**) Protein quantification of phospho-ERK, S6$^{S235/236}$ and S6$^{S240/244}$ in the DS (**A**) and NAc (**B**). For immunoblot pictures see **Suppl. Fig. 2C**. Statistics: *p<0.05,

p<0.01 and ***p<0.001, comparisons to control mice. (C, D**) Temporal profile of locomotor activity and cumulative locomotor response (**C^1** and **D^1**) of animals treated with the dopamine transporter blocker GBR during the anticipatory phase (**C**, **C^1**) or 1-hour after intermittent access to water (Ctr + GBR) or palatable diet (Binge + GBR) (**D**, **D^1**). Results are expressed as beam breaks (bb). Statistics: **p<0.01 Binge+GBR *vs* Control+GBR. (**E**) Palatable diet intake after vehicle (Veh+Binge) or D1R antagonist SCH23390 (SCH+Binge) pretreatment. Note: SCH23390 was acutely administered 30 min before binge session. Statistics: ***p<0.001 SCH+Binge *vs* Veh+Binge. (**F**) Palatable diet intake after vehicle (Veh+Binge) or D2R antagonist haloperidol 0.25 mg/kg or 0.5 mg/kg ($H^{0.25}$+Binge and $H^{0.5}$+Binge) treatment. Note: haloperidol was acutely administered 30 min before binge session. (**G**) Immunolabeling of phospho-S6 in the DS and NAc (for immunolabeling images of NAc see **Suppl. Fig. 2E**) and their associated quantifications (**G^1**, **G^2**, **H^1**, **H^2**) in mice pretreated with SCH23390 or vehicle and exposed to time-locked palatable diet. Scale bar: 50 µm. Statistics: ***p<0.001 Veh+Binge *vs* Veh+Control, $^{###}$p<0.001 SCH+Binge *vs* Veh+Binge. (**I**) Temporal profile of locomotor activity and cumulative locomotor response (**I^1**) of animals receiving SCH (SCH+Binge) or vehicle (Veh+Binge) (red arrow) and access to palatable diet (black arrow). Statistics: **p<0.01 SCH+Binge *vs* Veh+Binge. (**J**) Cumulative regular chow diet intake following acute SCH23390 (SCH+Binge) or vehicle (Veh+Binge). Statistics: **p<0.01 SCH+Binge *vs* Veh+Binge. (**K**) Temporal profile of locomotor activity and cumulative locomotor response (2 hrs and 30 min, **K^1**) induced by the D1R agonist SKF81297 administered 1 hour after access to time-locked water (Ctr+SKF) or palatable diet (Binge+SKF). Statistics: *p<0.05 and **p<0.01 Binge+SKF *vs* Control+SKF. For number of mice/group and statistical details see **Suppl. Table 1**.

Fig. 3: Peripheral endocannabinoids (eCBs) govern binge eating. (**A**) Palatable bingeing in animals pretreated (1h prior binge session) with vehicle (Veh), leptin, insulin, GLP1 agonists exendin-4 (Exe4) and liraglutide (Lira), CCK octapeptide sulfated (CCK-8S) or CB1R inverse agonist AM251. Aside leptin (2 injections/day for 2 consecutive days, **Suppl. Fig. 3A, B**), drugs were administered acutely. Statistics: ***p<0.001 Exe4-, Lira-, CCK-8S- & AM251-treated Bingeing mice *vs* Veh+Binge mice, $^{###}$p<0.001 AM251-treated *vs* Exe4-, Lira & CCK-8S-treated bingeing mice. (**B**) Dosage of peripheral and circulating endocannabinoids: anandamide (AEA),

diacylglycerol (2-AG), docosahexanoyl ethanolamide (DHEA) and oleoylethanolamide (OEA) 1 hour before and after palatable bingeing. (**C**) Palatable bingeing in mice (3 males and females/group) pre-treated with a single i.p. injection of vehicle (Veh), peripheral CB1R antagonist AM6545 (10 mg/kg) and peripheral CB1R inverse agonist JD-5037 (3 mg/kg). Statistics: ***p<0.001 AM6545 and JD-5037 *vs* Veh-Binge. (**D**) Palatable bingeing in mice pre-treated with a single i.p. injection of vehicle (Veh), peripheral CB1R antagonist AM6545 (10 mg/kg), and/or monoacylglycerol lipase inhibitor JZL184 (8 mg/kg). Statistics: ***p<0.001 AM6545, JZL184, AM6545+JZL184 *vs* Veh-Binge. (**E**) Chronic (4 days) administration of JZL184 and AM6545 on palatable bingeing. Statistics: ***p<0.001 AM6545-Binge *vs* Veh-Binge, ###p<0.001 JZL184-Binge *vs* Veh-Binge. (**F**) Effects of acute AM6545 on core temperature. Statistics: **p<0.01 AM6545-Binge *vs* Veh-Binge. Note: black and red arrows indicate administration of AM6545 and palatable food access, respectively. (**G**) Immunolabeling and quantifications of phospho-S6 and cFos in the DS and NAc of control or bingeing animals (males and females) acutely pretreated with Veh or AM6545. Scale bars: 50 µm. Statistics: ***p<0.001 and *p<0.005 Veh+Binge or AM6545+Binge *vs* Ctr, ###p<0.001 AM6545+Binge *vs* Veh+Binge. (**H**) Longitudinal measurement of fatty acid oxidation (FAO) following administration of AM6545 during a Binge session and a NoBinge session. (**H^1**) Averaged FAO from time of injection (11h00) till the end of light phase (19h00). (**H^2**) Ratio of FAO and food intake (FI) to discriminate between the effect of AM6545 and calories intake. Statistics: ***p<0.001 AM6545 *vs* Veh (in both Binge and NoBinge sessions). (**I**) Palatable bingeing after acute oral gavage of AM6545 (10 mg/kg, p.o.) and (**J**) associated fatty acid oxidation. (**K, L**) Immunolabeling and quantifications of cFos in the cNTS/AP regions (**K**) and in the lPBN (**L**) of control or bingeing animals (males and females) acutely pretreated with Veh or AM6545. Scale bars: 250 µm. Statistics: ***p<0.001, **p<0.01 and *p<0.005 Veh+Binge or AM6545+Binge *vs* Ctr, ###p<0.001 AM6545+Binge *vs* Veh+Binge. For number of mice/group and statistical details see **Suppl. Table 1**.

Fig. 4: The gut-brain vagal axis is required for eCBs-mediated effects. (**A**) The scheme indicates gut-originated afferent paths that were virally targeted to perform single-cell transcriptomic analysis [9]. (**B**) Enrichment of different vagal markers (*SLC17a6*, *Scn10a*, *Htr3a*, *Cartpt*, *Grin1*, *Phox2b*) and comparison with *Cnr1* and

Cnr2 in sensory vagal neurons labeled from microinjections in the stomach, proximal and middle intestines. Note: for other gut-brain vagal segments see **Suppl. Fig. 3H, I**. (**C**) Palatable food consumption in sham and vagotomized (VGX) animals pre-treated with Veh (Day 10) or JZL184 (Day 11-14) 2-hrs before bingeing sessions. Statistics: ***p<0.001 Sham+JZL184 *vs* Sham+Veh, $^{###}$p<0.001 VGX+JZL184 *vs* Sham+JZL184. (**D**) cFos immunolabeling in the area postrema (AP), caudal nucleus tractus solitarius (cNTS), lateral parabrachial nucleus (lPBN) and medial parabrachial nucleus (mPBN) in sham and vagotomized animals treated with the peripheral CB1R antagonist AM6545 (10 mg/kg). Scale bars: 250 µm. (**D^1**) Scheme indicates the central vagus→cNTS→PBN→target regions path in sham and VGX mice. (**D^2**) Quantification of cFos-positive neurons in the AP, cNTS and lPBN in sham and VGX mice injected with AM6545. Statistics: ***p<0.001 VGX+AM6545 *vs* Sham+AM6545. (**E**) Palatable bingeing in sham and vagotomized (VGX) animals pre-treated with AM6545 (A) or vehicle (V), and associated measurements of fatty acid oxidation (**F, F^1** and **G, G^1**). Statistics: ***p<0.001 Sham+AM6545 *vs* Sham+Veh. (**H, I**) cFos immunolabeling in the paraventricular nucleus (PVN) and dorsomedial nucleus of the hypothalamus (DMH) of sham or VGX animals acutely treated with vehicle or AM5646 and associated counting. Scale bars: 250 µm. Statistics: ***p<0.001 Sham+AM6545 *vs* Veh, $^{###}$p<0.001 VGX+AM6545 *vs* Sham+AM6545. For number of mice/group and statistical details see **Suppl. Table 1**.

Fig. 5: Peripheral CB1R signaling modulates dopamine dynamics. (**A, A^1**) Effect of AM6545 or Veh on GBR-induced locomotor activity (beam breaks, bb). Statistics: **p<0.01 AM6545+GBR *vs* Veh+GBR. (**B, B^1**) Effect of JD-5037 or Veh on GBR-induced locomotor activity. Statistics: **p<0.01, *p<0.05 AM6545+GBR *vs* Veh+GBR. (**C**) Effect of AM6545 on GBR-triggered cFos expression in the striatum. Scale bar: 50 µm. Statistics: ***p<0.001 AM6545+GBR *vs* Veh+GBR. (**D**) Longitudinal profile and heat maps of GBR-induced accumbal DA accumulation (dLight1.2) in mice pre-treated with Veh or AM6545 1h before GBR12909 (red arrow). (**D^1**) Quantification of bulk fluorescence (AUC) in Veh+GBR and AM6545+GBR groups. Statistics: ***p<0.001 AM6545+GBR *vs* Veh+GBR. (**E**) Cumulative locomotor activity response in mice pretreated with vehicle (Veh+Amph) or AM6545 (AM6545+Amph). For temporal locomotor activity see **Suppl. Fig. 6A**. (**F**) Cumulative locomotor activity response in mice pretreated with vehicle (Veh+Amph) or AM251 (AM251+Amph).

Statistics: ***p<0.001 AM251+Amph *vs* Veh+Amph. (**G**) GBR-induced locomotor activity, cumulative locomotor response (**G**[1]) in VGX mice pretreated with vehicle (VGX/Veh+GBR) or AM6545 (VGX/AM6545+GBR). (**H**) Cumulative locomotor response in mice pretreated with oral gavage (po) of vehicle (Veh (po)+GBR) or AM6545 (AM6545 (po)+GBR). For temporal locomotor activity see **Suppl. Fig. 6B**.

Fig. 6: Peripheral CB1R signaling routed by the vagus nerve controls VTA DA-neurons activity. (**A**) Expression of GCaMP6f in VTA DA-neurons of virally injected *Drd2*-Cre mice. Please, note (*i*) colocalization with TH and GCaMP6f-positive neurons and (*ii*) projecting terminals in the DS and NAc. See also, **Suppl. Fig. 6C** for TH expression in the VTA of *Drd2*-eGFP mice. (**B**) Behavioral paradigms used to trigger the activity of VTA DA-neurons: tail suspension and exposure to a new environment (NE). [For validation of *in vivo* recording of Ca^{2+} transients in VTA D2R-(DA)-neurons see **Suppl. Fig. 6D, E**]. (**C**, **D**) Temporal dynamics and corresponding heat maps of DA-neurons activity during the during the tail suspension test (**C**) and exposure to a new environment (**D**). Statistics: *p<0.05, **p<0.01 AM6545 *vs* Veh. (**E**) Immobility time (sec) of sham and VGX mice acutely pretreated with Veh or AM6545 1 hour before tail suspension (6 min). (**F**) Effect of AM6545 or Veh in sham and VGX mice on novel environment-induced locomotor activity. (**F**[1]) Cumulative locomotor activity response in sham and VGX mice pretreated with vehicle or AM6545. Statistics: **p<0.01 Sham/AM6545 *vs* Sham/Veh. (**G**) Cumulative locomotor activity response in sham and VGX mice pretreated with vehicle or AM251. Statistics: **p<0.01 Sham+AM251 *vs* Sham+Veh, and ##p<0.01 VGX+AM251 *vs* VGX+AM251. For number of mice/group and statistical details see **Suppl. Table 1**.

Figure 1 Berland et al.,

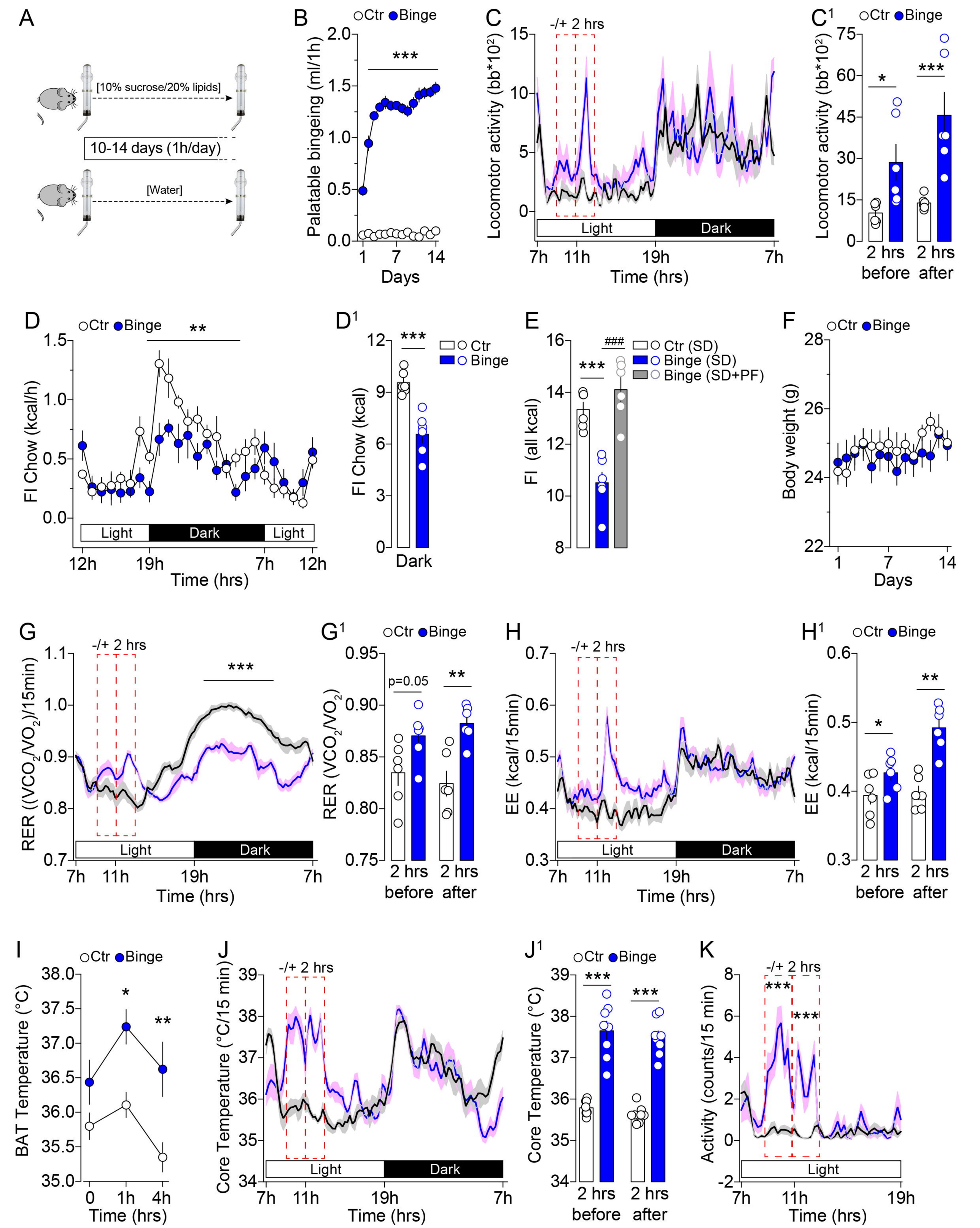

Figure 2 Berland et al.,

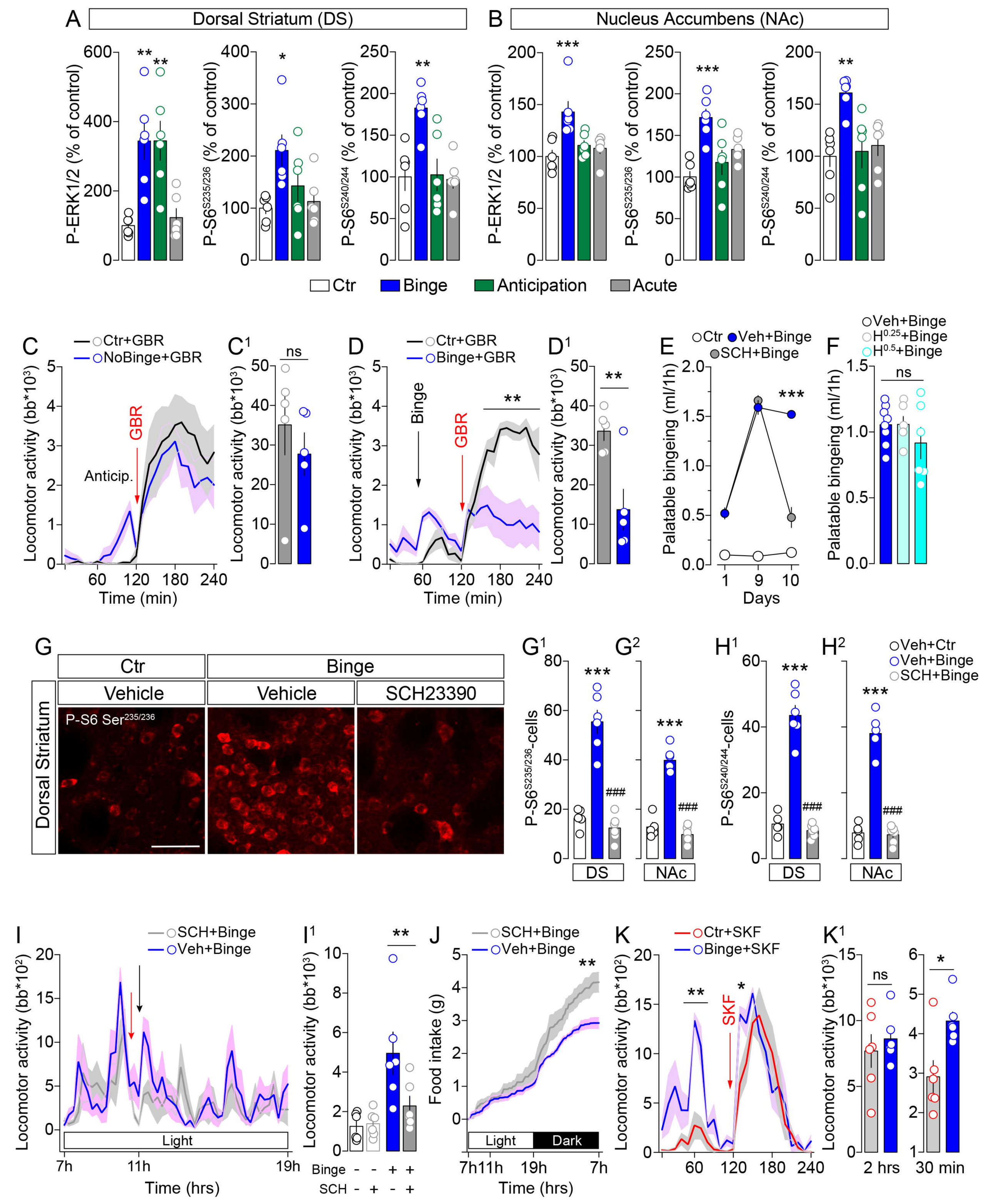

Figure 3 Berland et al.,

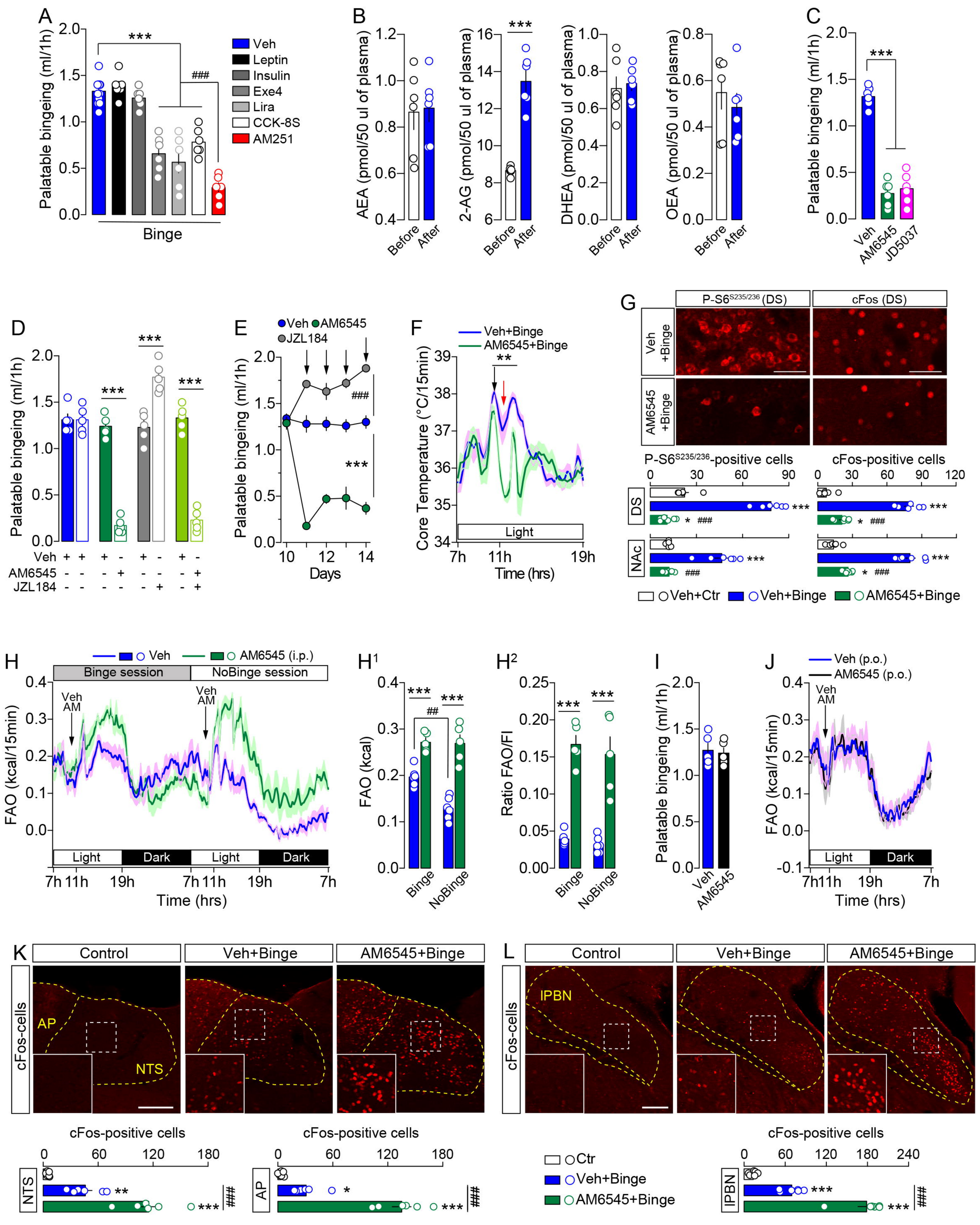

Figure 4 Berland et al.,

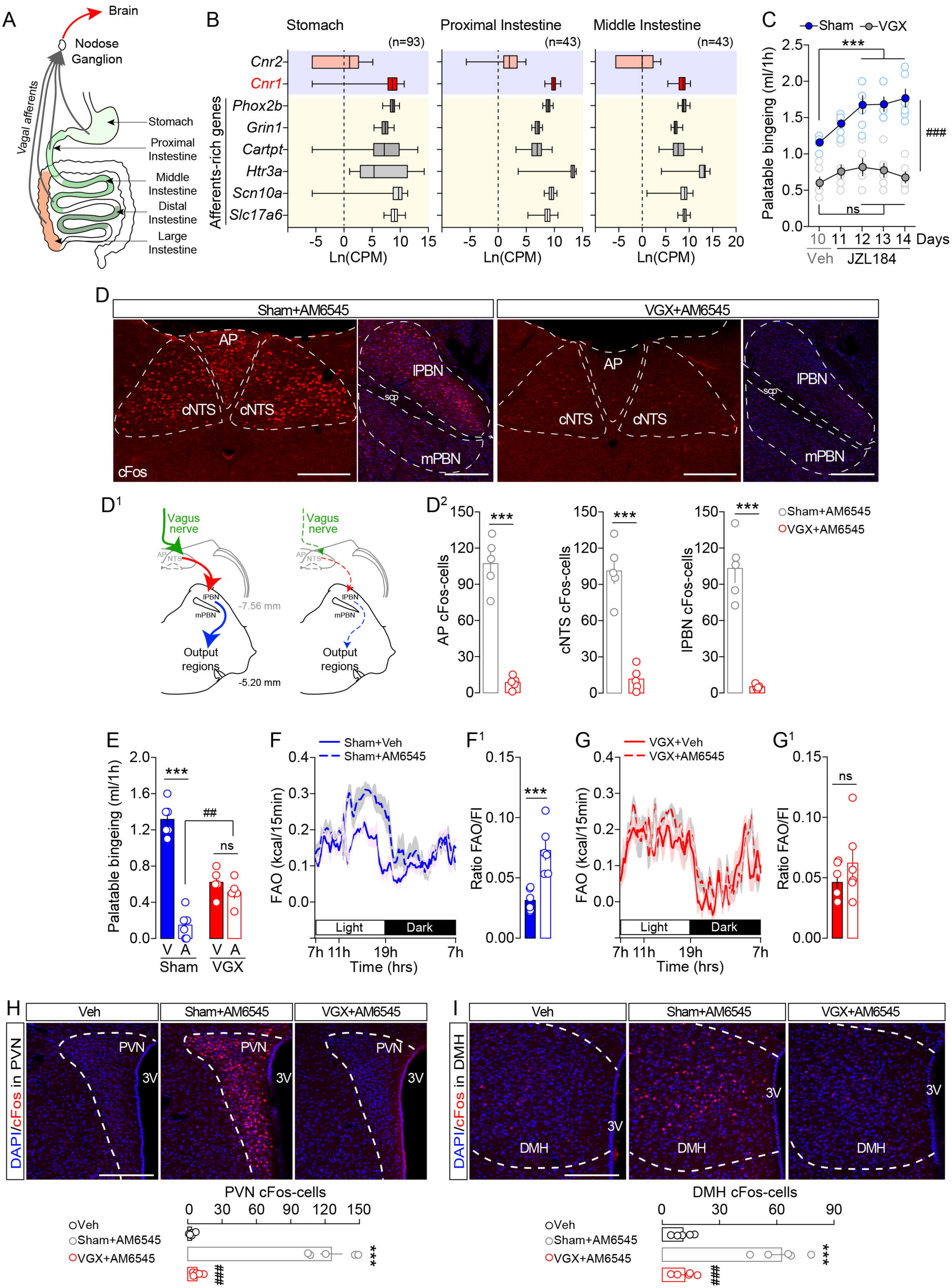

Figure 5 Berland et al.,

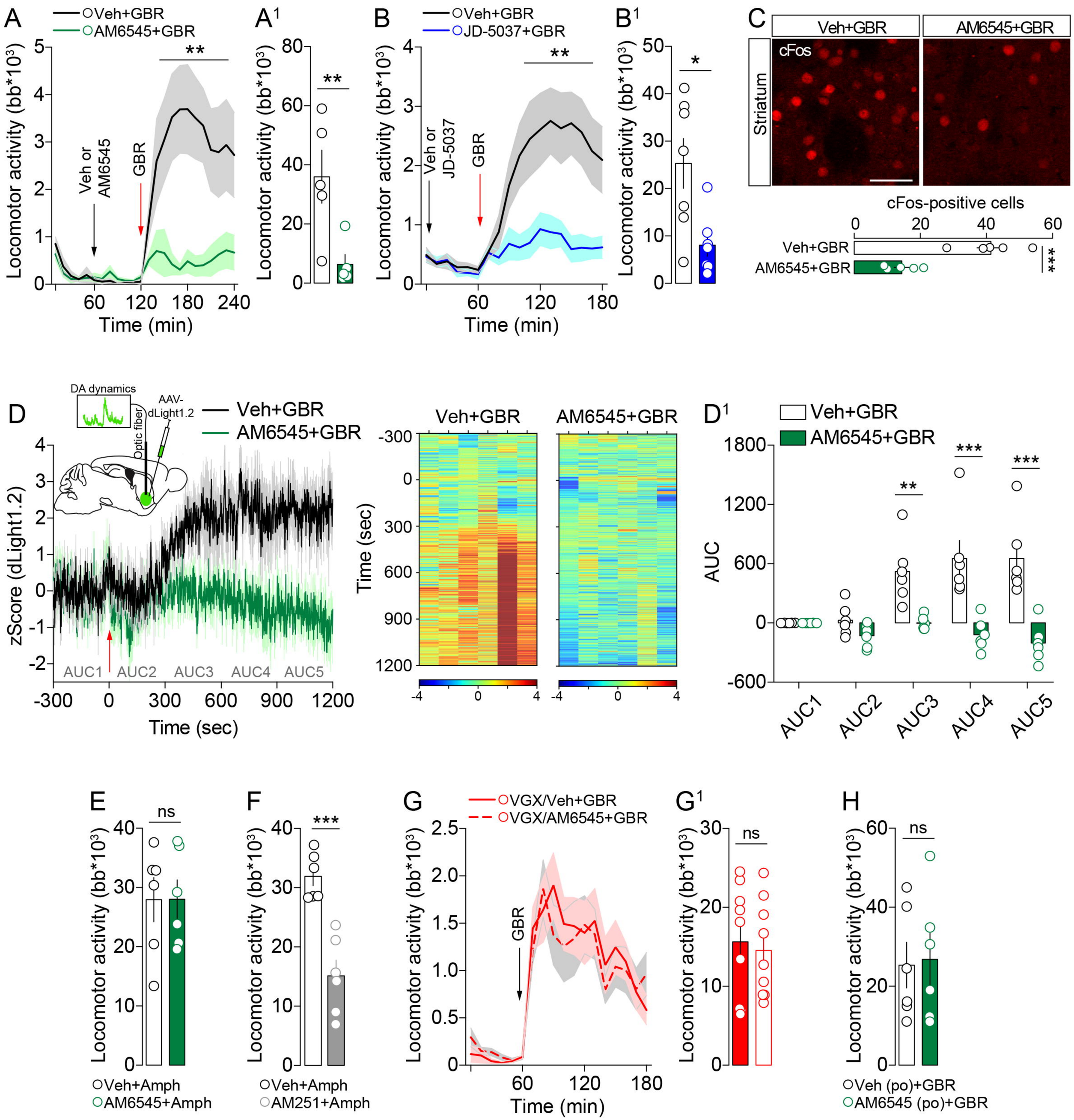
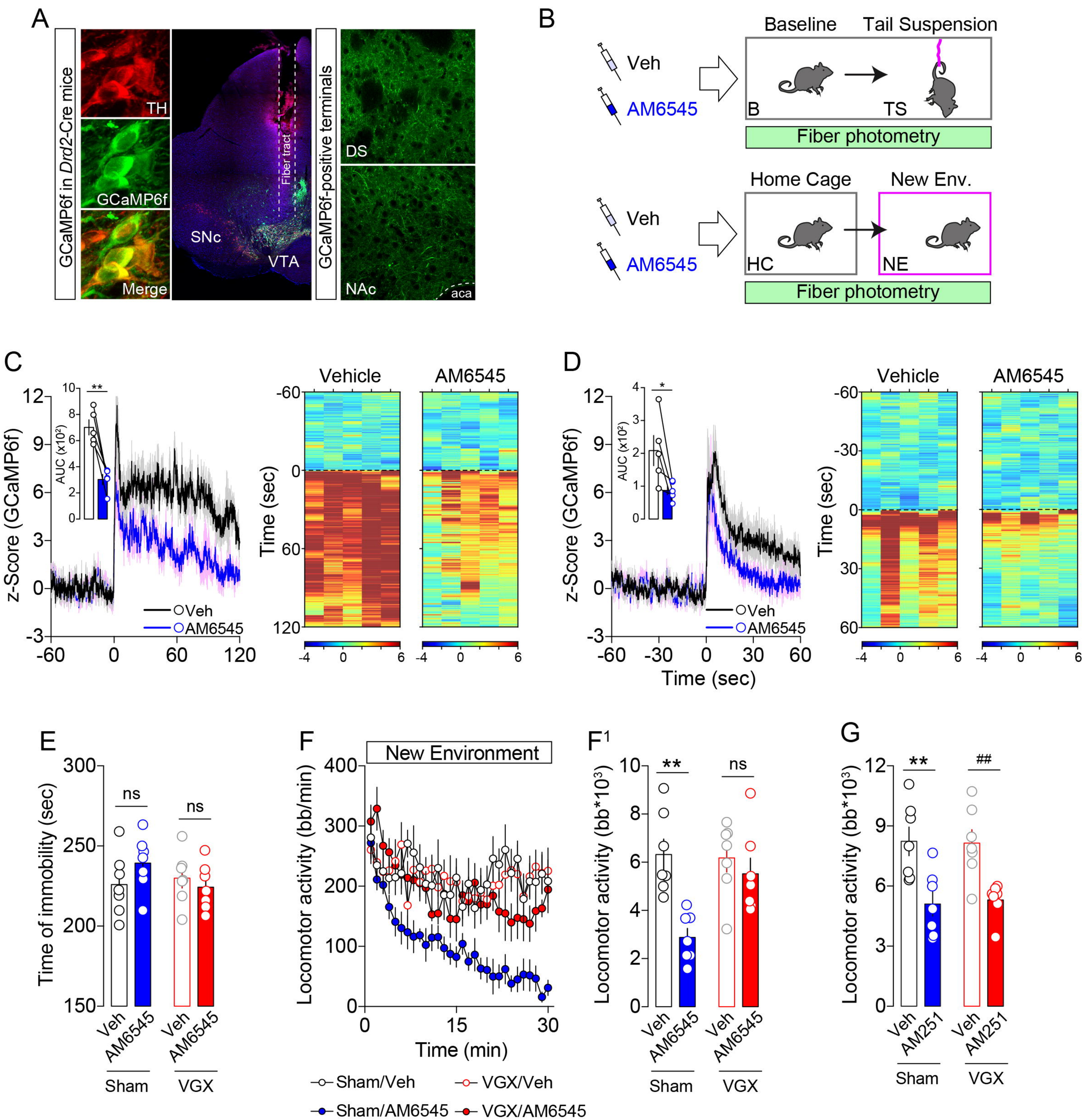
Figure 6 Berland et al.,